SIMULTANEOUS INVERSION OF RECEIVER FUNCTIONS, MULTI-MODE DISPERSION, AND TRAVEL-TIME TOMOGRAPHY FOR LITHOSPHERIC STRUCTURE BENEATH THE MIDDLE EAST AND NORTH AFRICA

Charles J. Ammon,[1] Robert B. Herrmann,[2] Michael E. Pasyanos,[3] William R. Walter,[3] Minoo Kosarian[1]

Penn State University,[1] Saint Louis University,[2] Lawrence Livermore National Laboratory[3]

Sponsored by Defense Threat Reduction Agency [1]
and
The National Nuclear Security Administration
Office of Nonproliferation Research and Engineering
Office of Defense Nuclear Nonproliferation[2,3]

Contracts No.: DTRA01-02-C-0038[1] & ROA01-31-LLNL[2,3]

ABSTRACT

We report on our initial investigations into the seismic structure of the lithosphere in the Middle East and North Africa using surface waves and receiver functions. We have initiated the collection of prior work in the region and computing receiver functions for use in the joint inversion. Critical to the joint inversion are surface-wave dispersion information localized to approximately the same region sampled by receiver functions. We continue to improve our surface wave dispersion model of Western Eurasia and North Africa. We have developed group velocity maps at 2-degree resolution for both Love and Rayleigh waves from 10- to 100-s period. The model shows excellent relationship to tectonic structure, and group velocity variations correlate well with orogenic zones, cratons, sedimentary basins, and rift zones. We have recently implemented a variable-resolution tomography and have pushed the resolution of the model down to 1 degree in areas with sufficient density sampling. We plan to present information on the complexity of receiver structure at many permanent sites in the region as well as several illustrative inversions for lithospheric structure. Other work on the combination of additional observations (body-wave travel times, higher-mode observations, surface-wave polarization information) is planned for the future stages of the project, but we include illustrations outlining our ideas for the use of these data to help further constrain the seismic structure of the lithosphere.

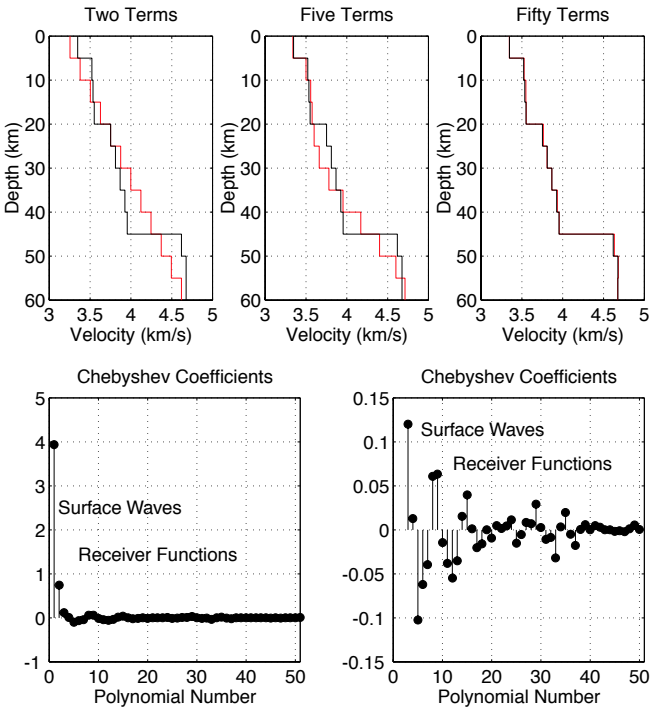

Figure 1. Expansion of a shear-velocity model (dark line in top panel) in terms of Chebyshev Coefficients. The top panel shows the sum of two, five and fifty terms respectively. The lower panels show the model spectra, that on the right focuses on the smaller amplitude, higher wave number coefficients. The point is that to image the structure, we must have data that can control the entire spectrum of the structure.

OBJECTIVES

Our objectives are the construction of shear-velocity profiles for regions surrounding broadband seismic stations throughout the Middle East, north Africa (MENA), central Africa, and parts of western Europe. Application of the technique in the MENA region provides an opportunity to revise models of the crust and upper mantle structure throughout the region and to exploit the global and regional work of previous seismic verification research (*e.g.* Pasyanos *et al.*, 2001; Ritzwoller & Levshin, 1998, Larson *et al.*, 2001). The resulting shear-velocity models provide a single structure consistent with a range of observations and which can be tested as a tool for the construction of mode isolation filters that can help improve surface-wave magnitude estimated. We also plan to explore the possibility of adding further data to our inversions of receiver functions, surface-wave dispersion. The diverse seismic activity throughout the region will facilitate cross-validation of the mode isolation filters with simple empirical filters constructed using larger events with adequate signal-to-noise ratios.

Background

Subsurface geology generally has a broad wave number spectrum (Figure 1) containing sharp, or high wave number, changes in velocity near Earth s major geologic boundaries and smooth low-wave number variations in regions of relatively uniform geologic structure. Access to the full spectrum of earth structure requires that we exploit signals that span a wide frequency range and that are sensitive to the entire spectrum of heterogeneity. Surface waves, travel times, and direct-wave amplitudes, for example, are sensitive to smooth variations in earth structure; reflected and converted waves are sensitive to velocity contrasts. Combining seismic data in joint inversions is an obvious approach to improve estimates of earth structure. To successfully combine data in an inversion, we must insure that all the data are sensitive to the same (or related) physical quantities and that they sample or average structure over comparable length scales. Recent advances in surface-wave tomography have provided an opportunity to combine localized surface-wave dispersion estimates with other data such as P- and S-wave receiver functions. Ammon and

Zandt (1993) used surface-wave dispersion observations to try and distinguish between competing models of the Mojave Desert, but zalaybey *et al.*, (1997) pioneered a formal, joint inversion of these data. They nicely illustrated the value of even a limited band of dispersion values to help reduce the trade-off between crustal thickness and velocity inherent in receiver function analyses. Specifically, they used Rayleigh-wave phase velocities in the 20- to 25-s period range to help produce stable estimates of crustal thickness in the northern and central Basin and Range. The limited bandwidth did not permit resolution of details in the crust and they limited their inversion (or at least their interpretation) to depths above 40 km. More recent authors have exercised the approach and combined the data with additional *a priori* model constraints (Du and Foulger, 1999; Julia *et al.*, 2000). Recent accomplishments in global and regional tomography now provide a more complete band of dispersion measurements to combine with receiver functions that allow us to improve the resolution of earlier works.

Surface-wave dispersion measurements are sensitive to broad averages, or low wave number components of earth structure. They provide valuable information on the absolute seismic shear velocity but are relatively insensitive to sharp, high-wave number velocity changes. Generally surface-wave inversions must be constrained using a particular layer parameterization (*e.g.* near-surface, upper-crust, lower crust, mantle lid, deep mantle), resemble an *a priori* model, or be substantially smoothed to stabilize earth-structure estimation. Despite these drawbacks, surface-wave dispersion values contain important constraints on the subsurface structure, and the general increase in depth sensitivity with depth allows an intuitive understanding of their constraints on structure. Additionally, modeling dispersion values facilitates a broadband inversion by reducing the dominance of Airy phases, which pose problems when constructing broadband misfit norms to model seismograms directly. Perhaps most important for our application is the ability to localize Earth s dispersion properties using seismic tomography. The idea is now well established, and global dispersion models exist for a broad range of frequencies (*e.g.* Larson and Ekstr m, 2001; Stevens *et al.*, 2001). The localization of dispersion allows us to isolate the variations in properties spatially, and global models of surface-wave dispersion exist and are readily available for application to other studies such as the proposed work.

Receiver functions are time/series computed from three-component body-wave seismograms, which show the relative response of Earth structure near the receiver (*e.g.* Langston, 1979). Source, near-source structure, and mantle propagation effects are removed from the seismograms using a deconvolution that sacrifices P-wave information for the isolation of near-receiver effects (Langston, 1979; Owens *et al.*, 1984; Ammon, 1991; Cassidy, 1992). Receiver function waveforms are a composite of P-to-S (or S-to-P) converted waves that reverberate within the structure near the seismometer. Modeling the amplitude and timing of those reverberating waves can supply valuable constraints on the underlying geology. In general, the receiver functions sample the structure over a range of tens of kilometers from the station in the direction of wave approach (the specific sample width depends on the depth of the deepest contrast). Stations sited near geologic boundaries can produce different responses for different directions. Recent innovations in receiver function analysis include more detailed modeling of receiver function arrivals from sedimentary basin structures (*e.g.* Clitheroe *et al.*, 2000), anisotropic structures (*e.g.* Levin and Park, 1997; Savage 1998), estimation of Poisson s ratio (*e.g.* Zandt *et al.*, 1995; Zandt and Ammon, 1995; Zhu and Kanamori, 2000, Ligorr a, 2000), reflection-like processing of array receiver functions (*e.g.* Chevrot and Girardin, 2000; Ryberg and Weber, 2000) and joint inversions (*e.g.* zalaybey *et al.*, 1997; Du and Foulger, 1999; Julia *et al.*, 2000).

Our joint inversion method is similar to that of zalaybey *et al.* (1997) except that we use jumping, smoothness, and constraints to include as much *a priori* information into the inversion as is available. We combine the receiver function and surface-wave observations into a single algebraic equation and account for their different physical units and equalize their importance in the misfit norm by weighting each data set by an estimate of the uncertainty in the observations and the number of data. We also append smoothness constraints and *a priori* model constraints on the deepest part of the model. Although we cannot resolve fine details in the deep upper mantle, these regions can impact our results since surface-wave dispersion values at intermediate and longer periods are somewhat sensitive to this deeper structure. We believe that it is important to have a reasonable basement structure so that our results are more consistent with global models. We extend our models to about 500—700*km* to insure this consistency. The resulting inversion equations are

$$\begin{bmatrix} \mathbf{p}\mathbf{D_s} \\ \mathbf{q}\mathbf{D_r} \\ \sigma\Delta \\ \mathbf{W} \end{bmatrix} \cdot \mathbf{m_{i+1}} = \begin{bmatrix} \mathbf{p}\mathbf{r_s} \\ \mathbf{q}\mathbf{r_r} \\ 0 \\ \mathbf{W}\mathbf{m_a} \end{bmatrix} + \begin{bmatrix} \mathbf{p}\mathbf{D_s} \\ \mathbf{q}\mathbf{D_r} \\ 0 \\ 0 \end{bmatrix} \cdot \mathbf{m_i} \qquad (1)$$

where $\mathbf{p}$, $\mathbf{q} = 1 - \mathbf{p}$, σ, and $\mathbf{W}$ are weights that control the relative importance of receiver functions, dispersion values, smoothness, and *a priori* model constraints in the norm minimized during the inversion. The data comprise the vectors $\mathbf{r_s}$ and $\mathbf{r_r}$, and the partial derivatives fill the matrices $\mathbf{D_r}$ and $\mathbf{Ds}$. The matrix Δ is a finite-difference stencil that computes model roughness, and the matrix $\mathbf{W}$ is a layer-dependent weight that is used to insure the model blends smoothly into the *a priori* model, $\mathbf{m_a}$, at depth. The second term on the right is added to create the jumping inversion scheme (*e.g.* Constable *et al.*, 1987; Ammon *et al.*, 1990) and allows us to solve for (and constrain) the shear-velocity models as opposed to shear-velocity correction vectors. Equation (1) is solved in a least-squares sense for the model, $\mathbf{m_{i+1}}$, starting with an initial model $\mathbf{m_0}$. The procedure generally converges in a few iterations.

RESEARCH ACCOMPLISHED

Receiver Function Computation

The first step in the project is the selection of target stations and the computation of receiver functions at those stations. To begin, we have selected a subset of permanent stations that have relatively long recording histories and thus will have substantial data already available. More recently installed stations and operating temporary stations will be added later in the project. Data processed at the time this report was written (July 2002) are shown in Figure 2. We plan to include all available temporary and permanent stations within central and northern Africa, the Middle East, and parts of Europe.

When the data are high quality and the receiver structure is not too complex, the choice of a deconvolution procedure does not make much difference. However, when the noise in the seismograms is substantial, or the receiver structure is complex, different deconvolution approaches have strengths and weaknesses. We will compute receiver functions using the iterative time-domain deconvolution procedure described by Ligorr a and Ammon (1999). We prefer the iterative approach, which is based on the Kikuchi and Kanamori (1982) source-time function estimation algorithm, for several reasons. First, in the iterative approach the receiver function is constructed by a sum of Gaussian pulses, which produces a flat spectrum at the longest periods. The flat long-period spectrum can be viewed as *a priori* information that helps reduce side-lobes that may result from spectral or singular-value truncation stabilization procedures. The reduction of side-lobes eases the interpretation and helps stabilize low-frequency receiver functions. Second, the iterative approach constructs a causal receiver function, which is what we expect in all cases of reasonable earth structure. This is a subtle difference from spectral techniques (*e.g.* Langston, 1979; Park and Levin, 2000) which can always introduce a component to the signal before the P-wave. The acausal component of the spectral signal may be small but still important to the satisfaction of the convolutional model that defines a receiver function, *i.e.:*

$$\mathbf{R}(\mathbf{t}) = \mathbf{Z}(\mathbf{t}) * \mathbf{E_R}(\mathbf{t}). \qquad (2)$$

In equation (2), $\mathbf{R}(\mathbf{t})$ and $\mathbf{Z}(\mathbf{t})$ are the radial and vertical seismograms, and $\mathbf{E_R}(\mathbf{t})$ is the radial receiver function (a similar equation holds for the transverse component). The point is that even when the receiver function estimation is unstable, spectral deconvolutions may satisfy (2) quite well. The iterative time-domain approach, which can be restricted to produce the best *causal* solution, may not always satisfy (2). Experienced modelers have always been able to identify failed receiver functions, but the misfit to (2) available from iterative deconvolutions provides quantitative information that can be used when stacking signals, or in extreme cases, to discard obviously failed deconvolu-

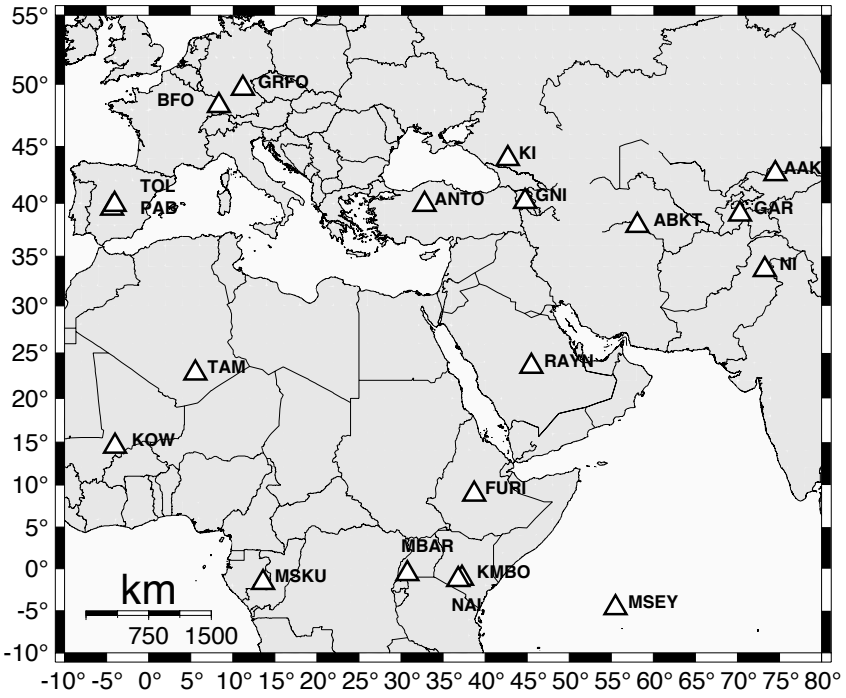

Figure 2. Stations for which we have already computed receiver functions (as of the date of this report). The eventual target stations include all available permanent and temporary three-component seismic stations.

tions. In our case we find using a threshold cut-off of 80-90% of the radial power fit allows us to quickly discard poorly constrained deconvolution results, enabling an efficient and objective selection of the data to include in further analysis.

Tomographic Imaging of Group-Velocity Variations

We have performed a large-scale study of surface wave group velocity dispersion across Western Eurasia and North Africa (Pasyanos, 2002). This study expands the coverage area northwards relative to previous work (Pasyanos *et al.*, 2001), which covered only North Africa and the Middle East. As a result, we have increased by about 50% the number of seismograms examined and group velocity measurements made. We have now made good quality dispersion measurements for about 10,000 Rayleigh wave and 6000 Love wave paths, and have incorporated measurements from several other researchers into the study. We use a conjugate gradient method to perform a group velocity tomography.

We have improved our inversion from the previous study by adopting a variable smoothness (Pasyanos, 2002). This technique allows us to go to higher resolution where the data allow without producing artifacts. Our current results include both Love and Rayleigh wave inversions across the region for periods from 10 to 100 s. Figure 3 shows inversion results for Rayleigh waves at periods of 20 and 50 s. Short-period group velocities are sensitive to slow velocities associated with large sedimentary features such as the Russian Platform, Mediterranean Sea, and Persian Gulf. Intermediate periods are sensitive to differences in crustal thickness, such as those between oceanic and continental crust or along orogenic zones. At longer periods, we find fast velocities beneath cratons and slow upper mantle velocities along rift systems and the Tethys Belt.

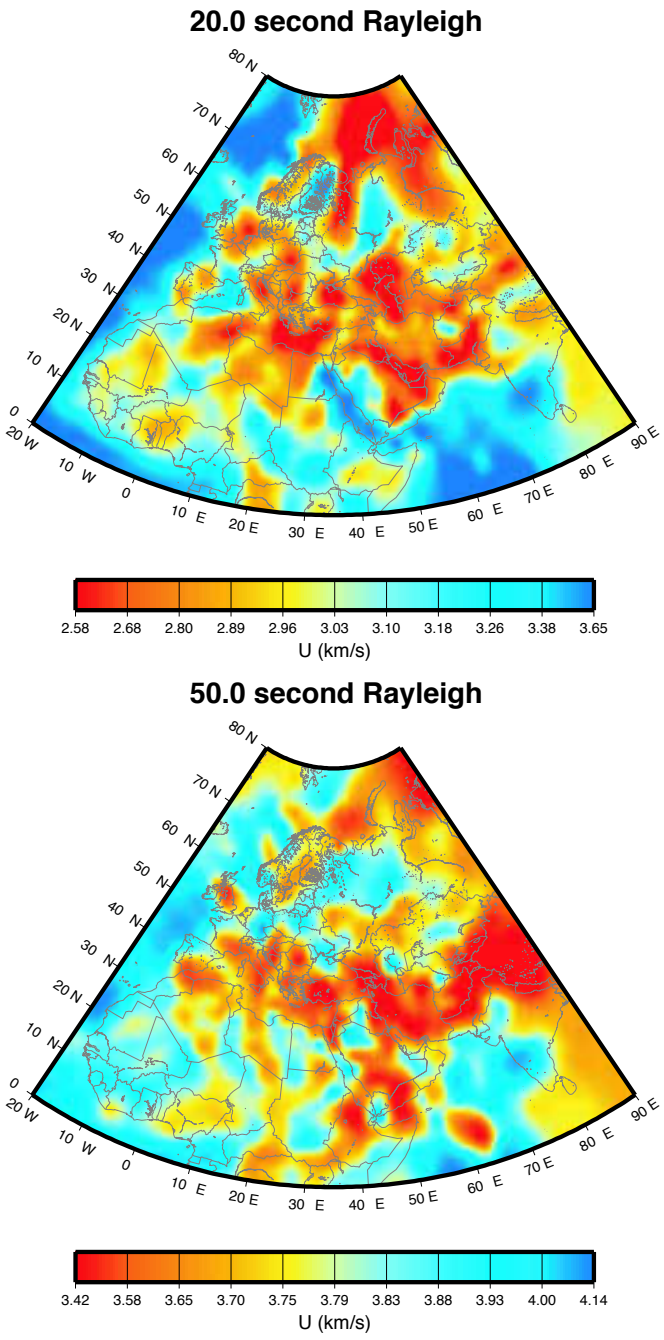

Figure 3. Tomographic imaging results for the Middle-East, North Africa, and western Europe. The upper diagram shows the lateral group velocity variations in 20-second period Rayleigh waves, the lower 50-second period Rayleigh waves.

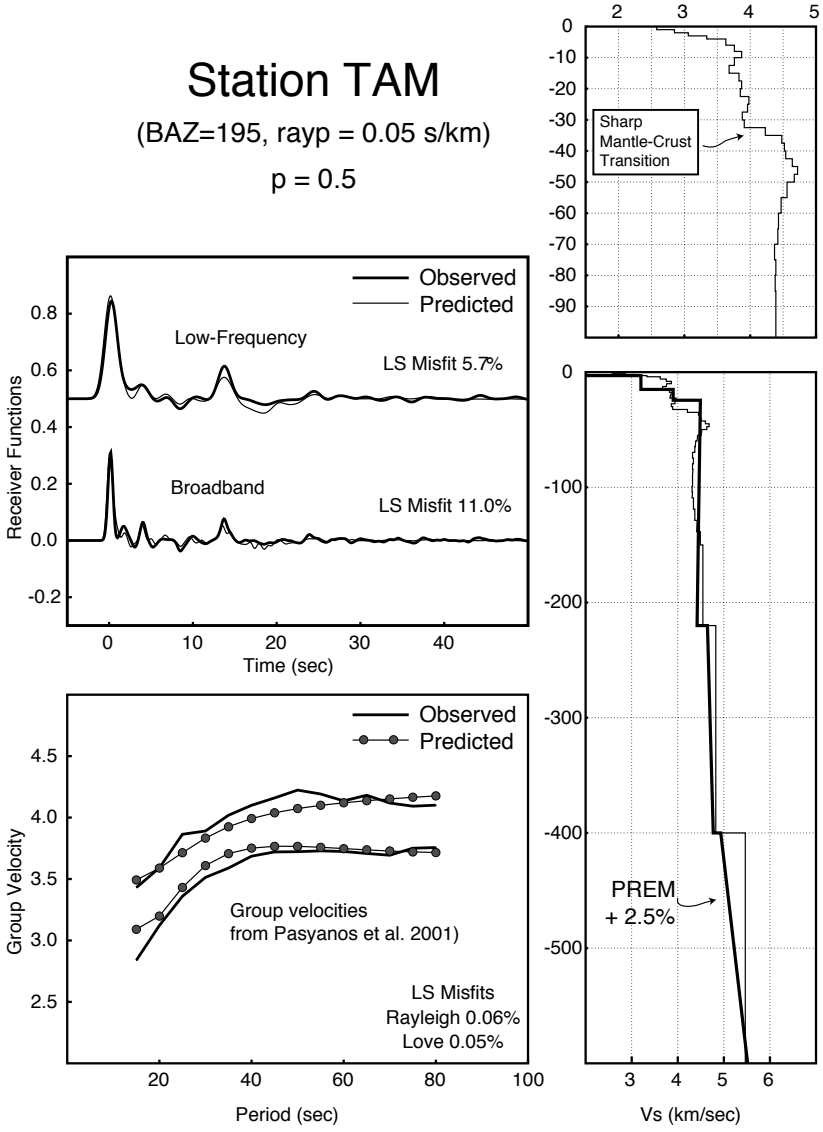

Figure 4. Preliminary inversion results for station TAM, located in north-central Africa. The receiver function in two bandwidths (low- and broad- frequency band) are inverted simultaneously to weight lower-frequency signals more. The group velocities from Pasyanos *et al.*, 2001 and the corresponding fits are shown on the lower left. The fit is generally good to all the observations although some systematic misfits between Love and Rayleigh wave dispersion are apparent. The structure is relatively simple and constrained to blend gradually into a modified PREM model.

An Example, Station TAM, North Africa

We illustrate the ideas with an example. We computed receiver functions for GEOSCOPE station TAM using events from the 1990 s. We extracted intermediate-period (period ‡ 12 s) group velocity dispersion measurements from the Lawrence Livermore National Laboratory (LLNL) MENA group velocity map (Pasyanos *et al.*, 2001). The joint inversion results for the station are shown in Figure 4. The observations are shown on the left, the models on the right. The receiver functions for this station are relatively simple, dominated by converted phases and a sharp multi-

ple from the crust-mantle transition. The results are not optimal in the sense that for the preliminary calculation we fixed the deepest parts of the model to resemble a coarsely-layered structure with a velocity of about 2.5% faster than PREM, which corresponds to the values in Harvard Shear-Wave Model S12WM13 (Su *et al.*, 1996). We can adapt the solution to match the IASPEI-91 model to be more consistent with body-wave travel times, or use velocity-depth profiles extracted from global aspherical models. The crustal velocity structure is a little rough, which reflects small arrivals in the broadband receiver function. The crust is also relatively thin, about 35 km, which is roughly consistent, but slightly thinner than the 38 –0.0 (< 1.0) km estimated by Sandvol *et al.*, (1998). The relatively slow shallow structure is dictated by the surface waves and is much slower than the values in MENA 1.1 region 5. Including local dispersion at shorter periods from paths of nearby earthquakes (of which there are few in this case) would help to verify these values.

CONCLUSIONS AND RECOMMENDATIONS

Since we have just begun work in this project in the last few months, conclusions and recommendations are premature.

ACKNOWLEDGEMENTS

We thank P. Wessel and W. H. F. Smith (1990), the authors of GMT for producing easy-to-use, quality software for making maps and charts.

REFERENCES

Ammon, C.J., G.E. Randall, and G. Zandt (1990), On the non-uniqueness of receiver function inversions, *J. Geophys. Res.*, **95**, 15303-15318.

Ammon, C.J. (1991), The isolation of receiver effects from teleseismic P waveforms, *Bull. Seism. Soc. Am.*, **81**, 2504-2510.

Ammon, C. J., and G. Zandt (1993), The receiver structure beneath the southern Mojave Block, *Bull. Seism. Soc. Am.*, **83**, 737-755.

Cassidy, J.F., Numerical experiments in broadband receiver function analysis, *Bull. Seismol. Soc. Am.*, **82**, 1453-1474, 1992.

Chevrot, S., and N. Girardin (2000), On the detection and identification of converted and reflected phases from receiver functions, *Geophys. J. Int.*, **141** (3), 801-808.

Clitheroe, G., O. Gudmundsson, and B.L.N. Kennett (2000), Sedimentary and upper crustal structure of Australia from receiver functions, *Australian Journal of Earth Sciences*, **47** (2), 209-216.

Constable, S.C., R.L. Parker, and C.G. Constable (1987), Occam's inversion: A practical algorithm for generating smooth models from electromagnetic sounding data, *Geophysics*, **52**, 289-300.

Du, Z.J. and G.R. Foulger (1999), The crustal structure beneath the northwest fjords, Iceland, from receiver functions and surface waves, *Geophys. J. Int.*, **139**, 419-432.

Julia, J., C. J. Ammon, R. B. Herrmann, and A. M. Correig (2000), Joint Inversion of receiver function and surface-wave dispersion observations, *Geophys. J. Int.* **143**, 99-112.

Kikuchi, M., and H. Kanamori, Inversion of complex body waves (1982), *Bull. Seism. Soc. Am.*, **72**, 491-506, 1982.

Langston, C.A. (1979), Structure under Mount Rainier, Washington, inferred from teleseismic body waves, *J. Geophys. Res.*, **84**, 4749-4762.

Larson, E. W. F. and G. Ekstr m (2001), Global Models of Group Velocity, *Pure and Applied Geophys.*, **158**, 1377-1399.

Levin, V., and J. Park (1997), Crustal anisotropy in the Ural Mountains from teleseismic receiver functions, *Geophysical Research Letters*, **24** (11), 1283-1286.

Ligorr a, J.P. (2000), An Investigation of the Crust-Mantle Transition Beneath North America and the Bulk Composition of the North American Crust, *Ph.D. Thesis, Saint Louis University*, 261 pages.

Ligorr a, J.P. and C. J. Ammon (1999), Iterative deconvolution and receiver function estimation, *Bull. Seismol. Soc. Am.*, **89**, 1395-1400.

Myers, S.C., and S.L. Beck (1994), Evidence for a local crustal root beneath the Santa Catalina metamorphic core complex, Arizona, *Geology*, **22**, 223-226.

Owens, T.J., G. Zandt, and S.R. Taylor (1984), Seismic evidence for an ancient rift beneath the Cumberland Plateau, Tennessee: A detailed analysis of broadband teleseismic P waveforms, *J. Geophys. Res.*, **89**, 7783-7795.

zalaybey, S., M.K. Savage, A.F. Sheehan, J.N. Louie, and J.N. Brune (1997), Shear-wave velocity structure in the northern Basin and Range Province from the combined analysis of receiver functions and surface waves, *Bull. Seismol. Soc. Am.*, **87**, 183-199.

Park, J., and V. Levin (2000), Receiver functions from multiple-taper spectral correlation estimates, *Bull. Seismol. Soc. Am.*, **90** (6), 1507-1520.

Pasyanos, M.E., W.R. Walter, and S.E. Hazler (2001), A Surface wave dispersion study of the Middle East and North Africa for Monitoring the Comprehensive Nuclear-Test-Ban Treaty, *Pure and Applied Geophys*, **158**, 1445-1474.

Pasyanos, M.E. (2002), A Variable-resolution Surface Wave Dispersion Study of Western Eurasia and North Africa, submitted to *Journal of Geophysical Research*.

Ritzwoller, M. H. and A. L. Levshin (1998), Eurasian surface wave tomography: Group velocities, *J. Geophys. Res.,* **103**, 1839-1878.

Ryberg, T., and M. Weber (2000), Receiver function arrays; a reflection seismic approach, *Geophys. J. Int.*, **141** (1), 1-11.

Sandvol, E., D. Seber, A. Calvert, M. Barazangi (1998), Grid search modeling of receiver functions: Implications for crustal structure in the Middle East and North Africa, *J. Geophys. Res.*, **103**, 26,899-26,917.

Savage, M.K. (1998), Lower crustal anisotropy or dipping boundaries? Effects on receiver functions and a case study in New Zealand, *J. Geophys. Res.*, **103** (7), 15,069-15,087, 1998.

Stevens, J. L. and K. L. McLaughlin (2001), Optimization of Surface Wave Identification and Measurement, *Pure and Applied Geophys*., **158**, 1547-1582

Su, W., R. L. Woodward, and A. M. Dziewonski (1994), Degree 12 model of shear velocity heterogeneity in the mantle, *Nature*, **99**, 6945-6980.

Zandt, G., and C. J. Ammon (1995), Continental Crustal composition constrained by measurements of crustal Poisson's ratio, *Nature*, **374**, 152-154.

Zandt, G., S.C. Myers, and T.C. Wallace (1995), Crust and mantle structure across the Basin and Range-Colorado Plateau boundary at 37 degrees N latitude and implications for Cenozoic extensional mechanism, *J. Geophys. Res.*, **100** (6), 10,529-10,548.

Zhu, L., and H. Kanamori (2000), Moho depth variation in Southern California from teleseismic receiver functions, *J. Geophys. Res.*, **105** (2), 2969-2980.